Global perturbation in initial geometry in a biomechanical model of cortical morphogenesis

Amine Bohi

Institut de Neurosciences de la Timone, CNRS UMR 7289
Aix-Marseille Université (AMU)

Shape Analysis in Biology
21-22 nov. 2019 Paris

3D model of a real human brain. *Zbrush, 3DsMax (Vray)*

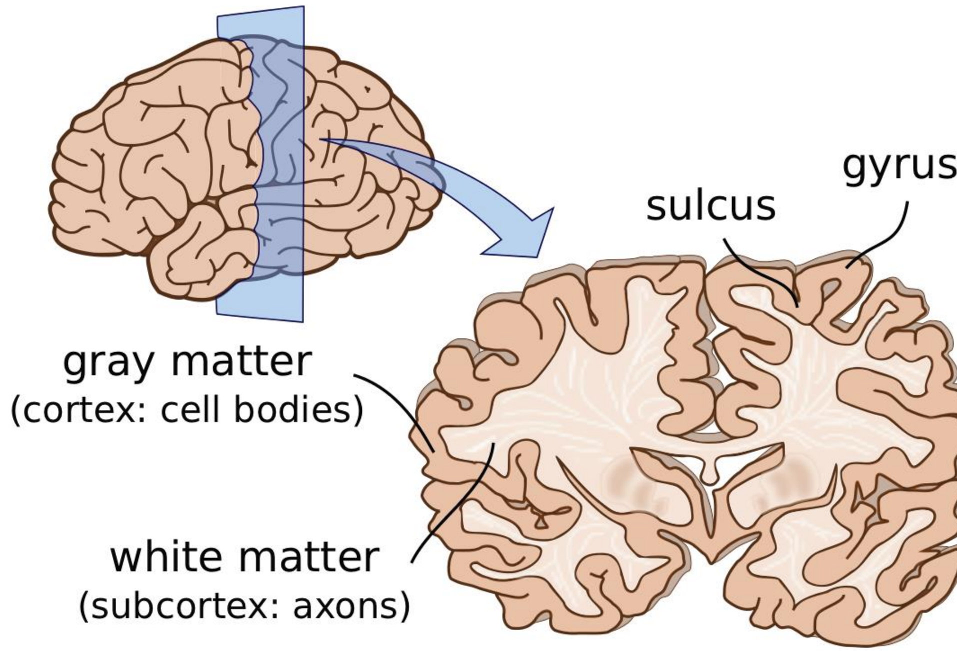

Schematic illustration of the human brain. *S. Budday et al. 2014*

Fetal brain normal development with dramatic changes in size and shape between 20 and 40 weeks

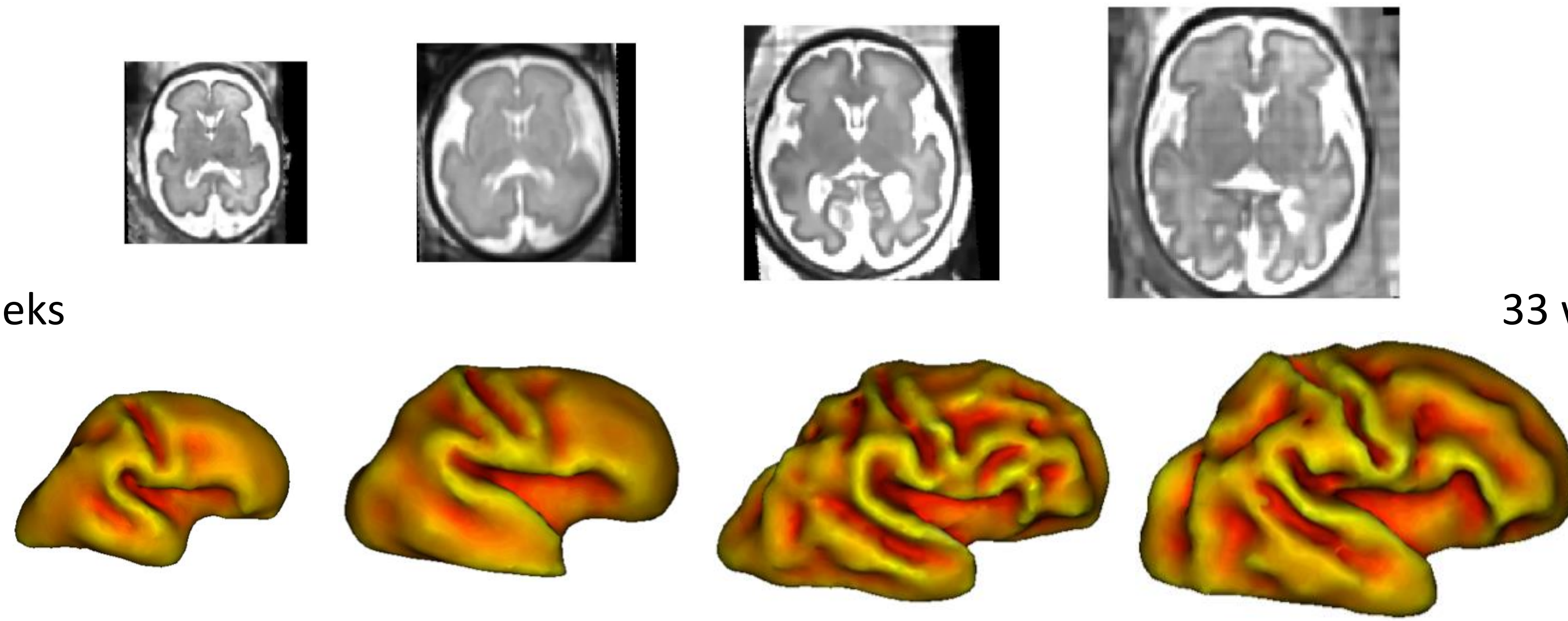

28 weeks

33 weeks

Fetal 2D images and reconstructed cortical meshes with the curvature coded in color at different gestational ages. Sulci are in red while gyri are in yellow. *Lefèvre et al. 2015*

Fetal brain normal development with dramatic changes in size and shape between 20 and 40 weeks

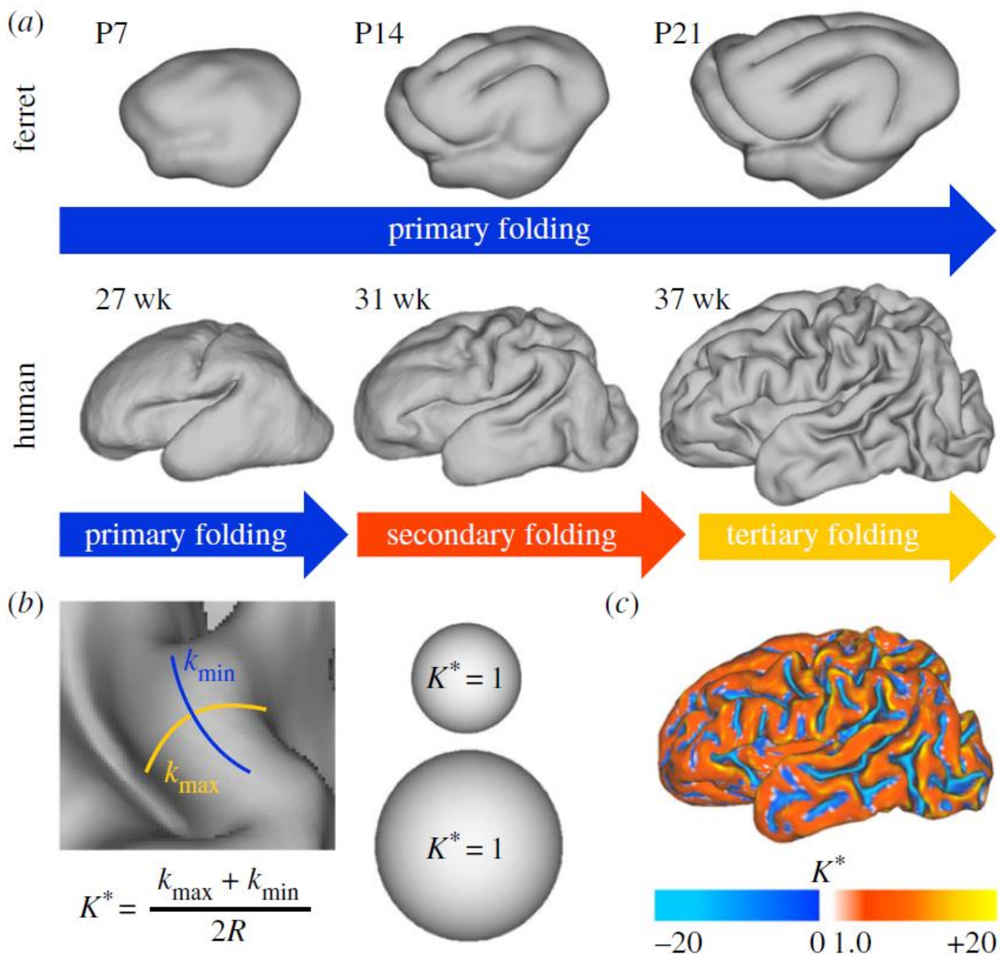

Measuring cortical folding. K.E. Garcia *et al. 2018*

- **Cortical folding ⟷ Overall size of the brain**

Porthero al al. 1984

Toro et al. 2008

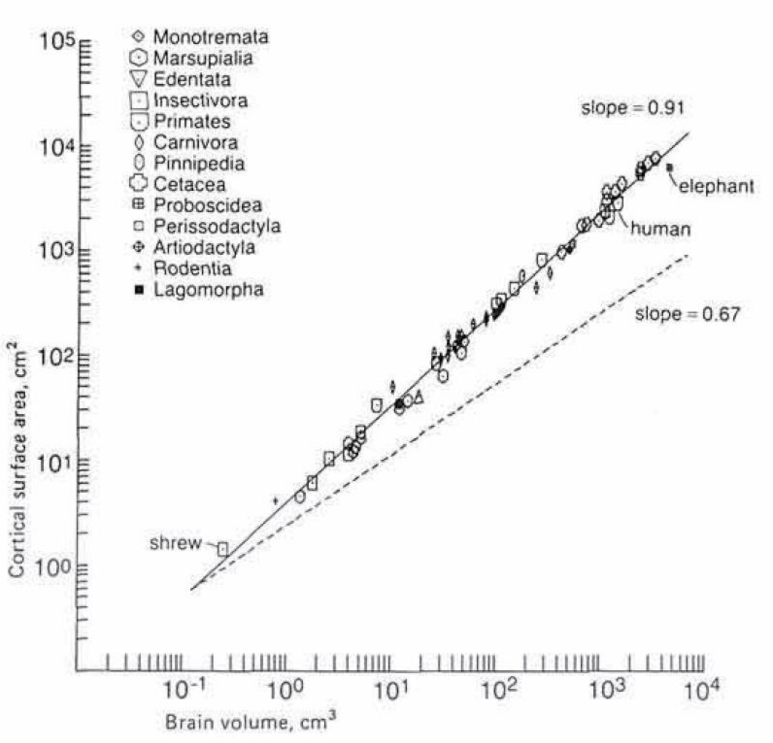

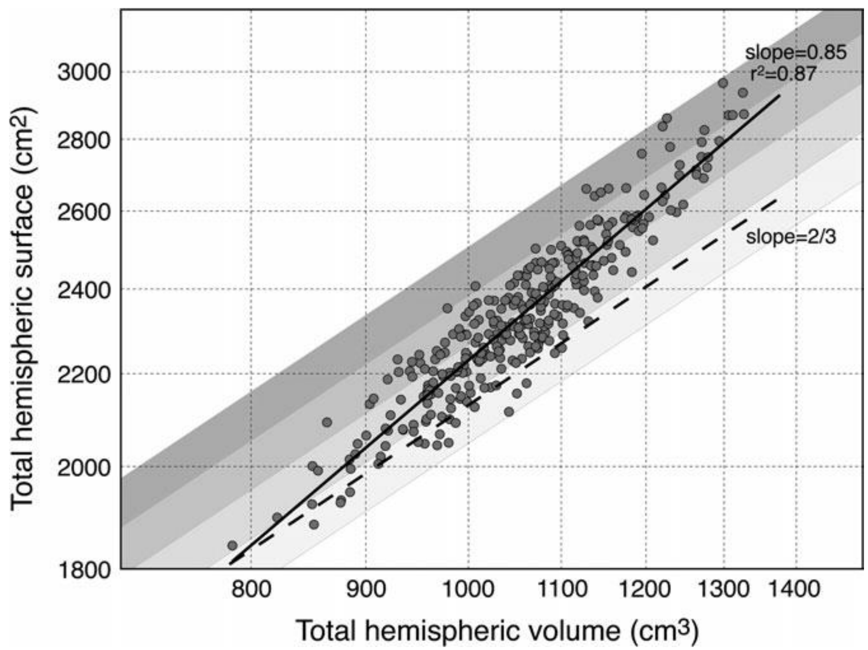

Cortical surface versus hemispheric volume.

- **Cortical folding ⟷ Overall size of the brain**

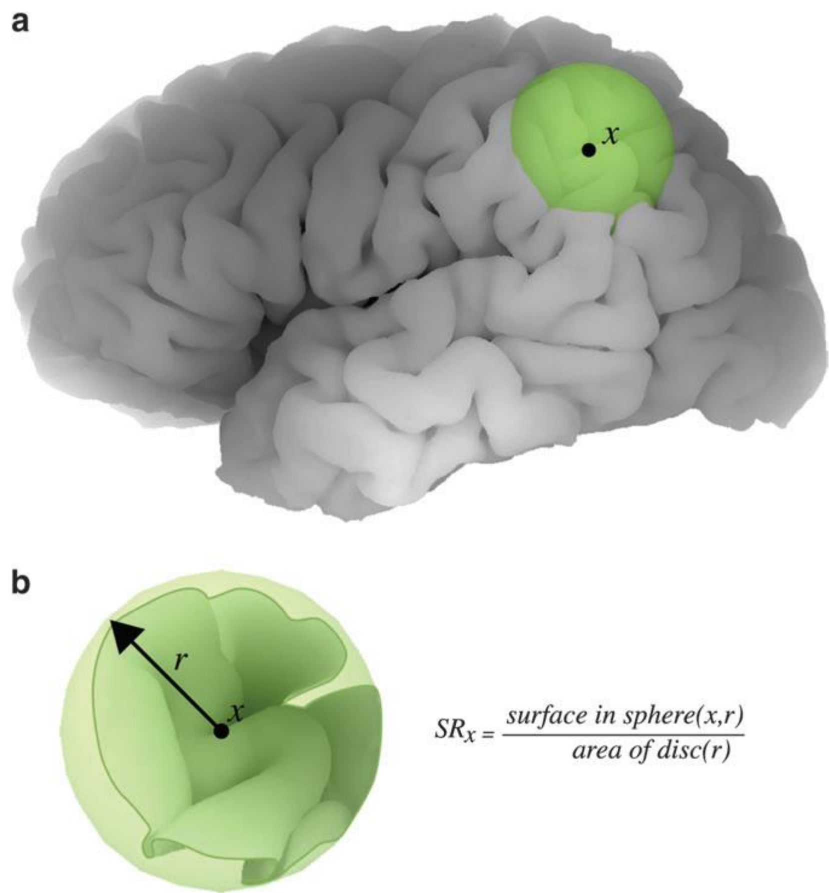

Surface ratio for the local estimation of folding. *Toro et al. 2008*

- **Cortical folding ⟷ Overall size of the brain**

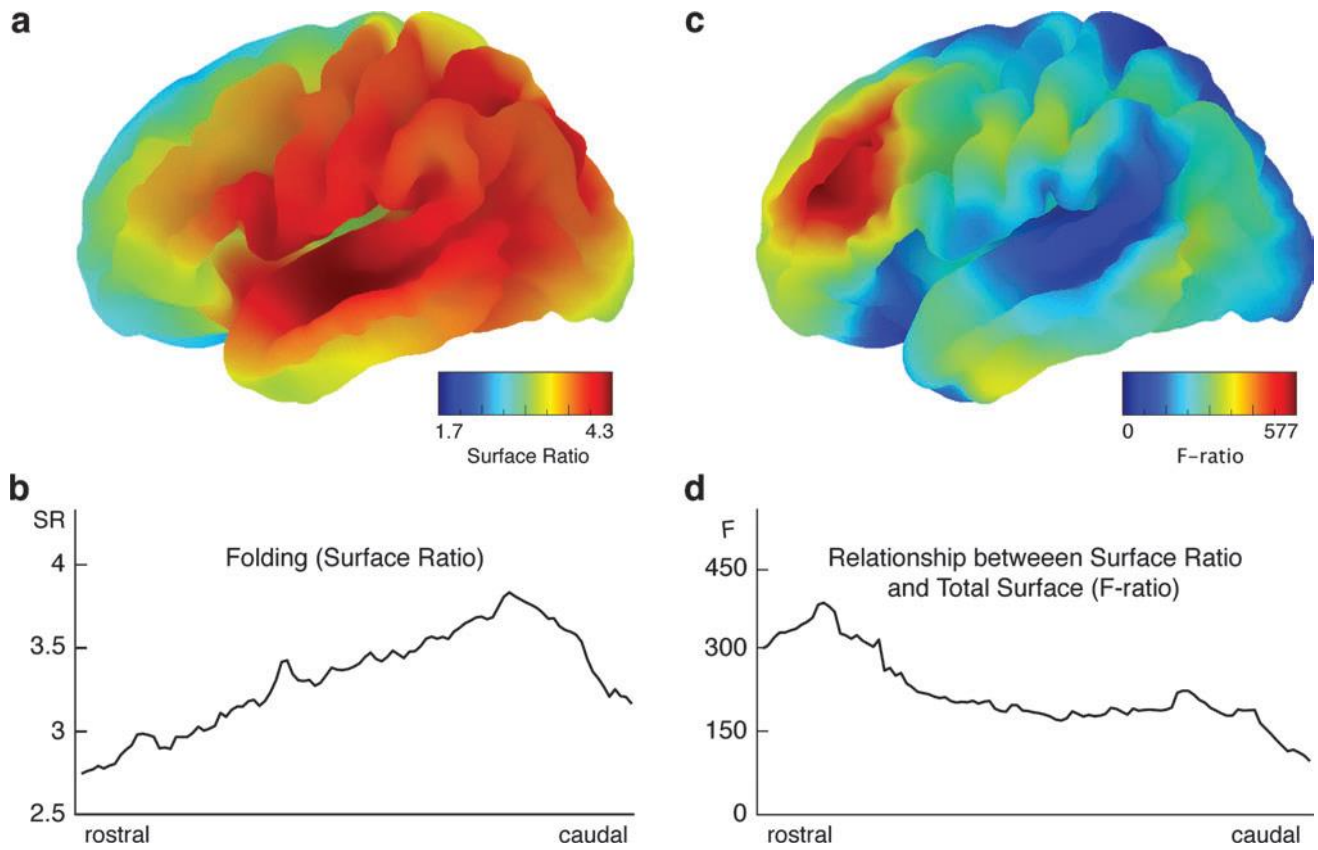

Map of average cortical folding (surface ratio) and significance of the effect of total cortical surface on local folding (F-ratio values). *Toro et al. 2008*

- Cortical folding ⟷ Overall size of the brain
- Can be modified by brain developmental disorders

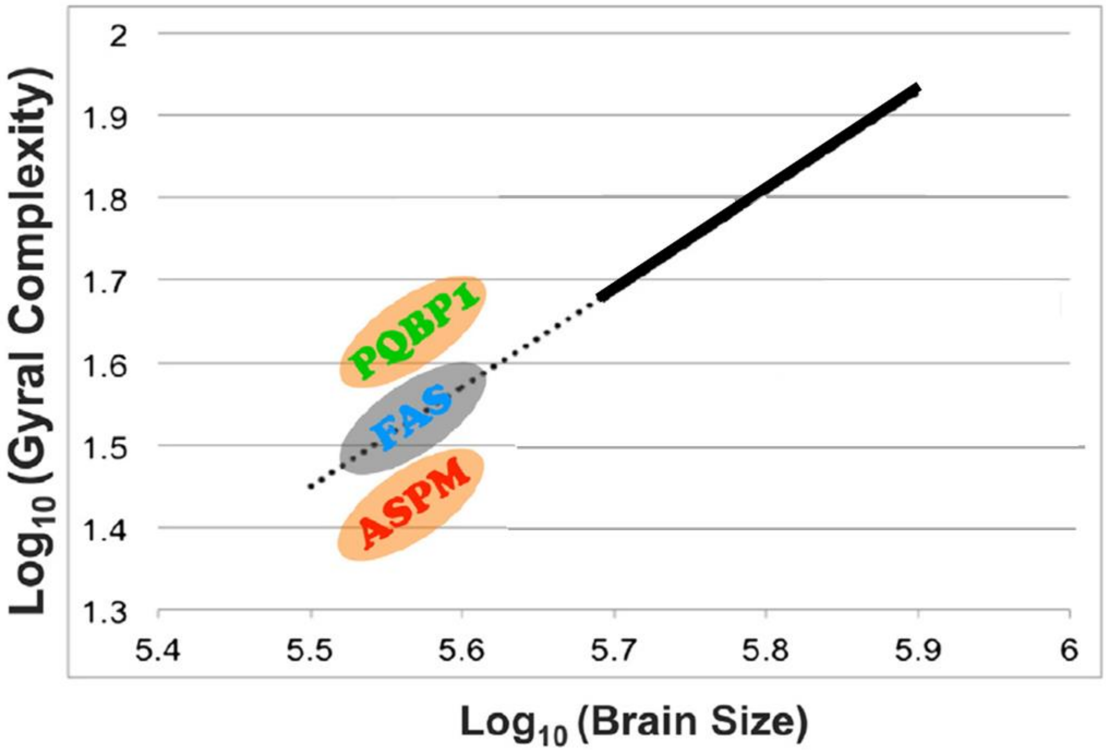

Microcephaly 270 cm³

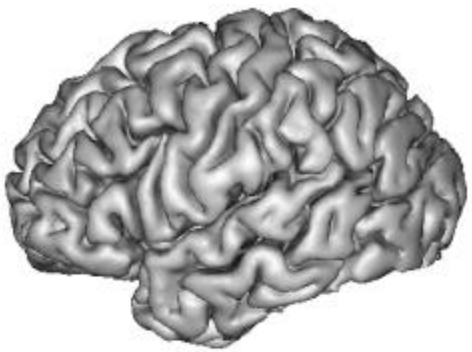

Control 445 cm³

Gyrification differences observed between a typically developing brain and severe microcephalies. *Germanaud et al. 2014*

Study the impact of the initial geometry of the human fetal brain on surface morphology during the cortical development process.

Using an adapted spherical parameterization to compare several cortical surfaces of fetal brains generated by the biomechanical model based on the finite element model of differential cortical and subcortical growth introduced in (Tallinen et al., 2016).

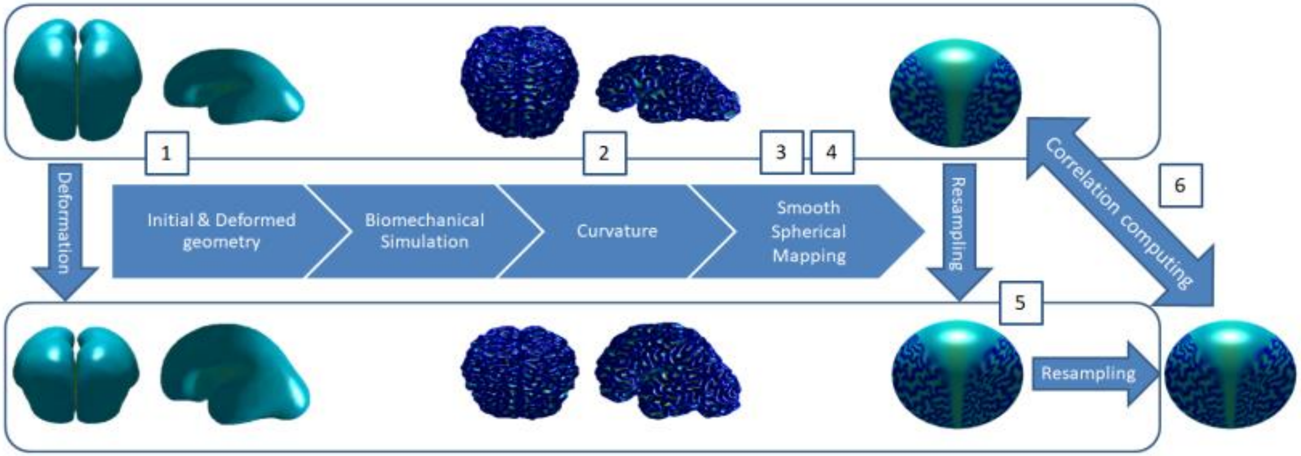

A. Bohi et al. 2019

❑Biomechanical modeling

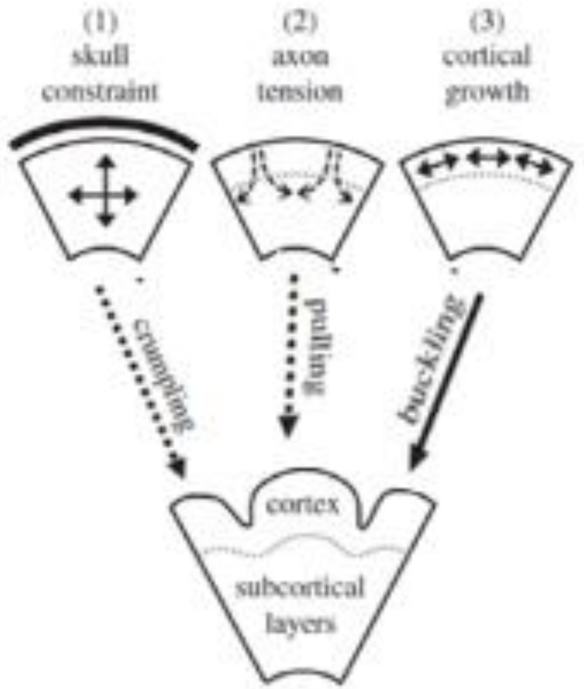

Competing hypotheses for cortical folding. *K. E . Garcia et al. 2018*

❑Biomechanical modeling

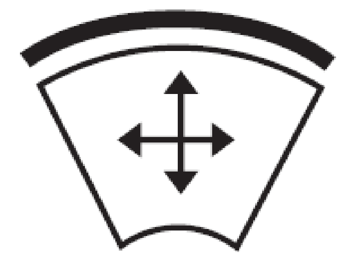

- A plate or shell-like structure, expanding tangentially inside a rigid container (skull), would have to fold
- The skull Constraints growth of the brain and causes compressive stresses and buckling. *Raghavan et al. 1997*
- *Barron 1950* : showed that interactions with skull are not needed to produce folding.
- *Welker 1990* : The skull increases in size to accommodate brain growth.

→ The role of skull in cortical folding has largely been discounted

❑Biomechanical modeling

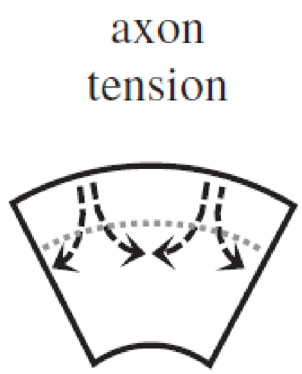

- Tension in axons connecting adjacent regions of the cortex draws those regions together to form gyri. *Van Essen, 1997*
- *Xu et al. 2010* : the observed directions of tension are not consistent with the original axonal tension hypothesis

→ Axons pull on the brain, but tension does not drive cortical folding

❑Biomechanical modeling

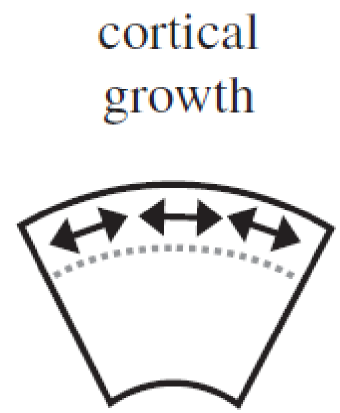

- Tangential expansion of outer cortical layers, greater than in inner layers, causes folding by a mechanical instability → meaning different growth rates in different layers. *Richman et al. 1975*
- Based on 2 mechanical principles :
  1- Tangential expansion of an elastic layer connected to an elastic foundation which does not expand → induces tangential compression in the expanding layer
  2- A thin layer under large compression → will become unstable and buckle (sinusoidal shape)
- Other models : *Toro & Burnod 2005, Bayly et al. 2013, Budday et al. 2014,* <u>*Tallinen et al. 2014 & 2016*</u>

→Validated by physical experiments of *Dervaux and Ben Amar 2008, Xu et al. 2010*, and <u>*Tallinen et al. 2016*</u>

❑Biomechanical modeling

cortical growth

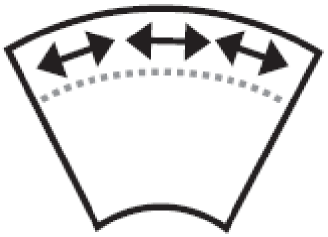

- Tangential expansion of outer cortical layers, greater than in inner layers, causes folding by a mechanical instability

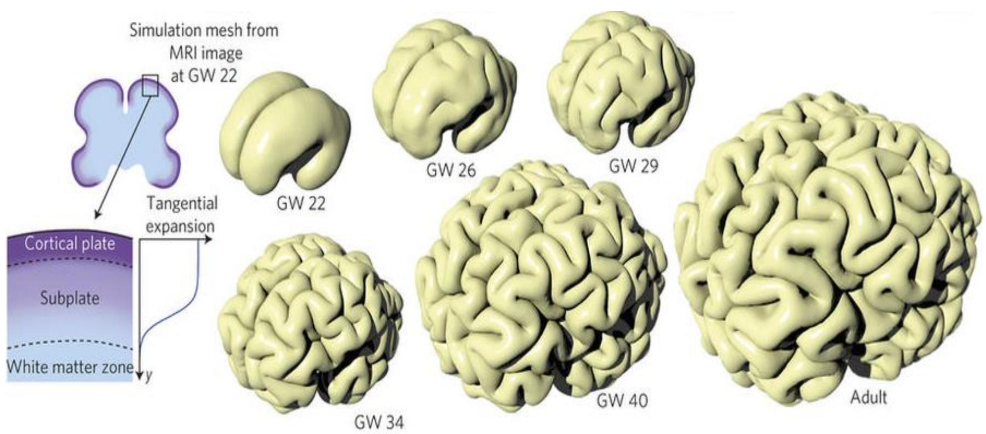

Differential growth of two layers. (*Tallinen et al. 2016*)

- **Growth tensor:**

$$g(y) = 1 + \frac{\alpha}{1 + e^{(10(\frac{y}{T}-1))}}$$

$$G = gI + (1-g)n_s \otimes n_s$$

- **Deformation gradient**

$$F = A(GA_r)^{-1}$$

- **Volumetric strain energy density**

$$W = \frac{\mu}{2}\left[T_r(FF^T)J^{\frac{-2}{3}} - 3\right] + \frac{K}{2}(J-1)^2$$

- **Cauchy stress**

$$\delta = \frac{1}{J}\frac{\partial W}{\partial F}F^T$$

❑Spherical parameterization for genus zero surfaces using Laplace-Beltrami eigenfunctions

Definitions :

- **Given an eigenfunction ϕ of the Laplace-Beltrami operator, we call *nodal set* the set of points $N(\phi)$ where ϕ vanishes.**
- **The nodal domains correspond to the connected components of the complementary of the nodal set.**

Theorem (Courant's nodal domain theorem):

- **The number of nodal domains for the n-th eigenfunction is inferior or equal to $n + 1$ (Neuman boundary conditions).**

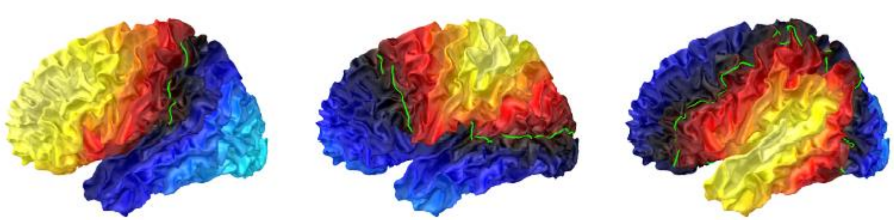

Three first non-trivial eigenfunctions. Each nodal lines are in green. (*Lefèvre et al., 2015*)

❑Spherical parameterization for genus zero surfaces using Laplace-Beltrami eigenfunctions

<u>Conjecture</u> (*Lefèvre et al. 2015*) : Let M be a genus zero surface in $\mathbb{R}^3$. Let ϕ_1, ϕ_2 and ϕ_3 be three non-trivial orthogonal eigenfunctions of the Laplace-Beltrami operator. We assume they have only two nodal domains. Then the mapping

$$\begin{array}{ccccc} \mathbf{M} & \to & \mathbb{R}^3 & \to & \mathbb{S}^2 \\ p & \to & (\Phi_1(p), \Phi_2(p), \Phi_3(p)) & \to & \dfrac{(\Phi_1(p), \Phi_2(p), \Phi_3(p))}{\sqrt{\Phi_1(p)^2 + \Phi_2(p)^2 + \Phi_3(p)^2}} \end{array}$$

is well defined.

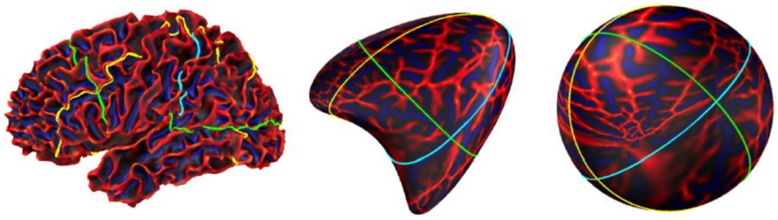

Spherical mapping. (*Lefèvre et al., 2015*)

❑Spherical parameterization for genus zero surfaces using Laplace-Beltrami eigenfunctions

<u>**Important remark**</u> **:**

- **The number of nodal domains must be 2.**
- **For elongated shapes, the bounds in Courant's nodal theorem are reached.**

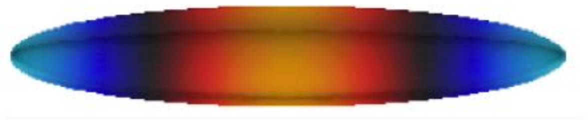

Φ_2

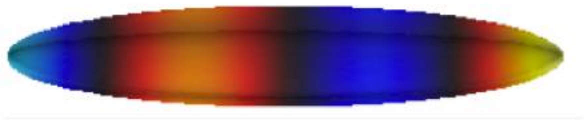

Φ_3

Some complex surfaces are unsuitable because they do not satisfy the conditions proposed in the previous conjecture

Generalizing the previous conjecture assuming that, for a genus-zero surface, we can always find three eigenfunctions associated to larger eigenvalues in the spectrum with only two nodal domains, which allows to provide a better spherical mapping

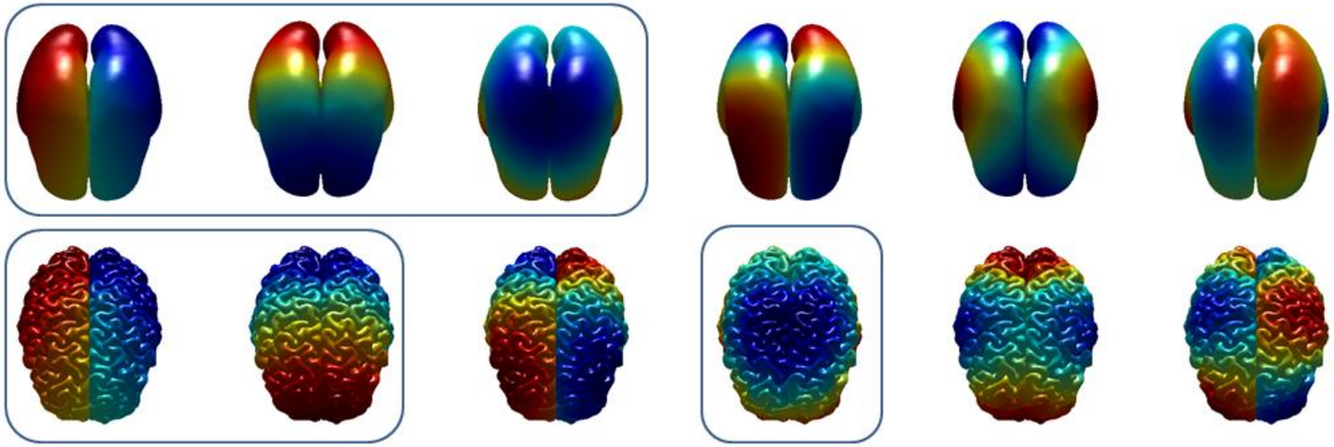

Six first eigenfunctions for a smooth fetal brain (first row) and a simulated cortex (second row). *A. Bohi et al. 2019*

STEP 1:

$$B_{ref} \xrightarrow{\quad M_{a,b} \quad} B_{a,b}, \quad \text{with} \quad M_{a,b} = \begin{pmatrix} a & 0 & 0 \\ 0 & b & 0 \\ 0 & 0 & c \end{pmatrix}$$

$$(B_{ref}, B_{a,b}) \xrightarrow{\quad \text{Biomechanical Model} \quad} (S_{ref}(t), S_{a,b}(t))$$

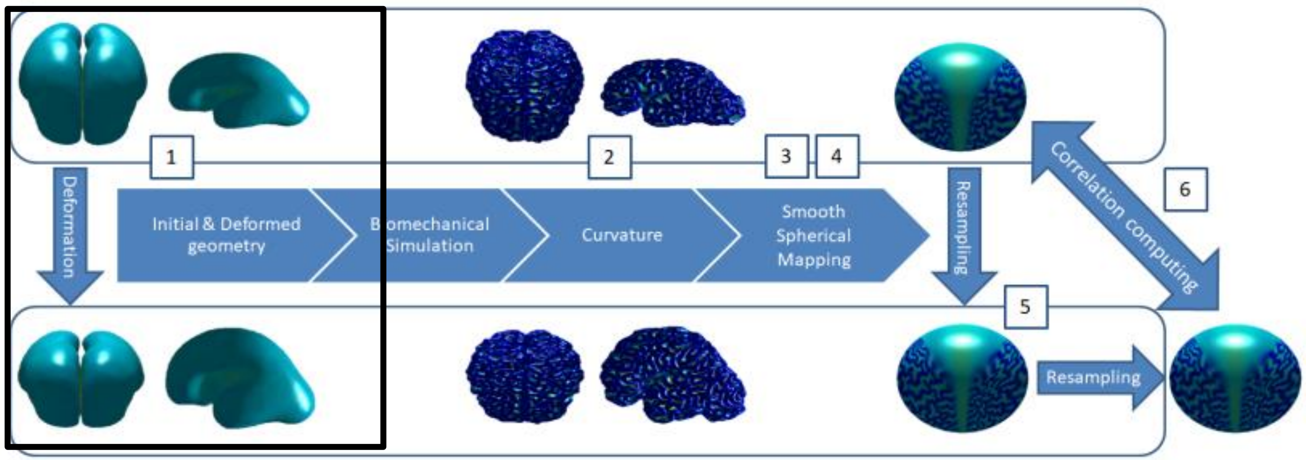

STEP 1:

$$B_{ref} \xrightarrow{M_{a,b}} B_{a,b}, \quad \text{with} \quad M_{a,b} = \begin{pmatrix} a & 0 & 0 \\ 0 & b & 0 \\ 0 & 0 & c \end{pmatrix}$$

$$(B_{ref}, B_{a,b}) \xrightarrow{\text{Biomechanical Model}} (S_{ref}(t), S_{a,b}(t))$$

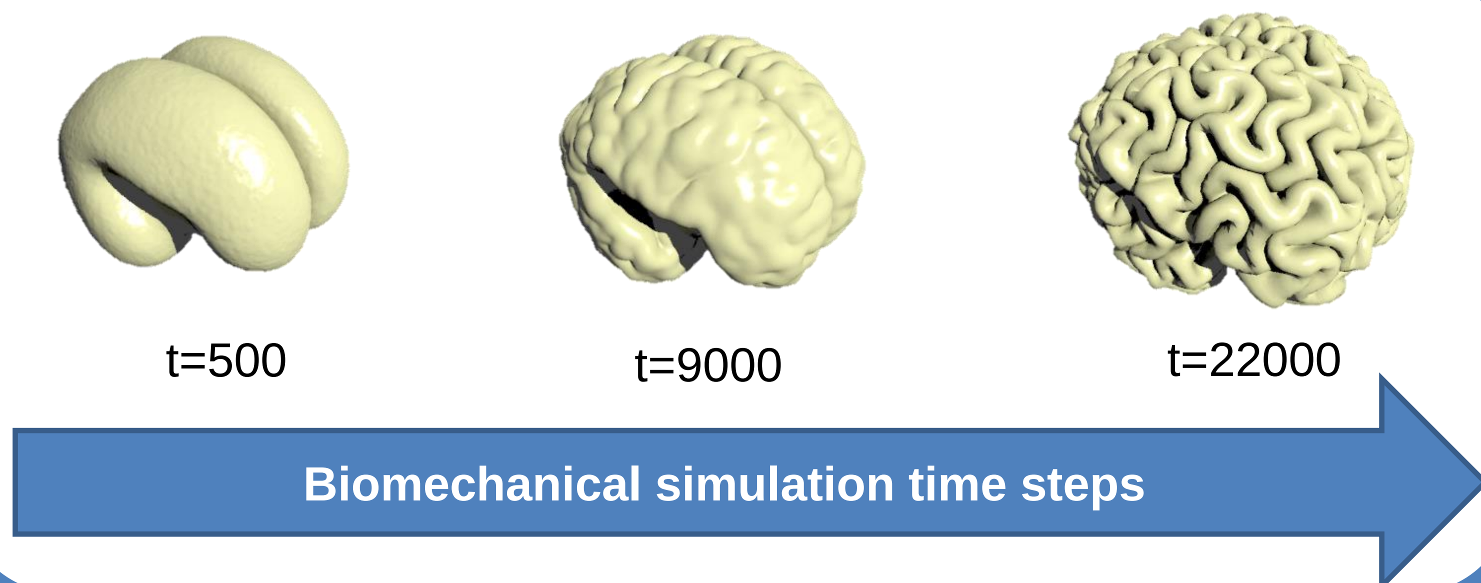

STEP 2 & 3:

Compute and smooth curvatures of $S_{ref}(t)$ and $S_{a,b}(t)$

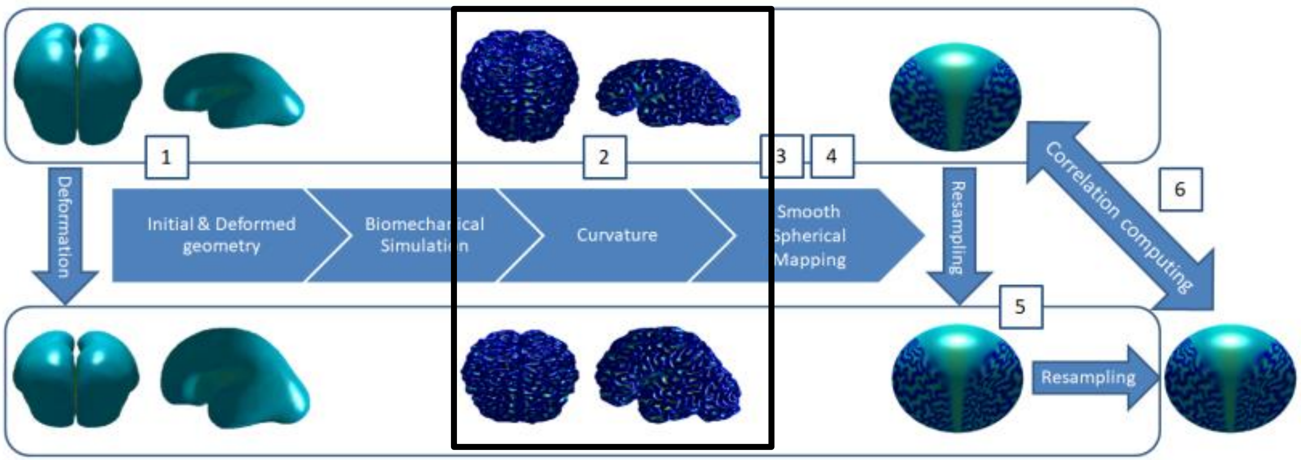

STEP 4:

The spherical mapping is, then, defined by selecting the best three non-trivial eigenfunctions with only two nodal domains, from a larger set of eigenfunctions of the Laplace-Beltrami operator of $S_{ref}(t)$ and $S_{a,b}(t)$.

$$S_{ref}(t), S_{a,b}(t) \rightarrow \mathbb{R}^3 \rightarrow \mathbb{S}^2$$

$$p \rightarrow (\Phi_1(p), \Phi_2(p), \Phi_3(p)) \rightarrow \frac{(\Phi_1(p), \Phi_2(p), \Phi_3(p))}{\sqrt{\Phi_1(p)^2 + \Phi_2(p)^2 + \Phi_3(p)^2}}$$

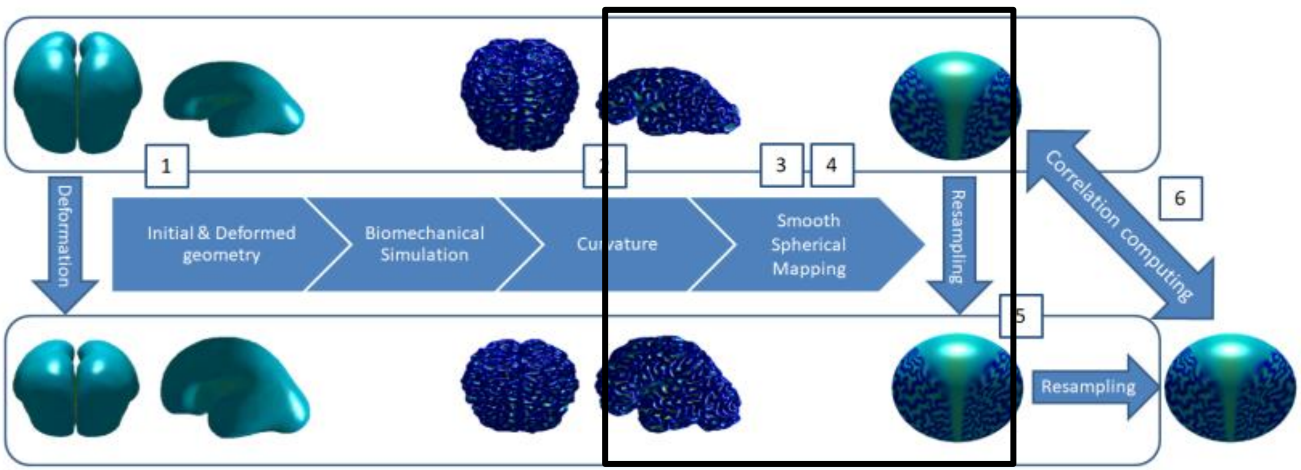

STEP 5:

Resample the curvature of the spherical map of $S_{ref}(t)$ on that of $S_{a,b}(t)$.

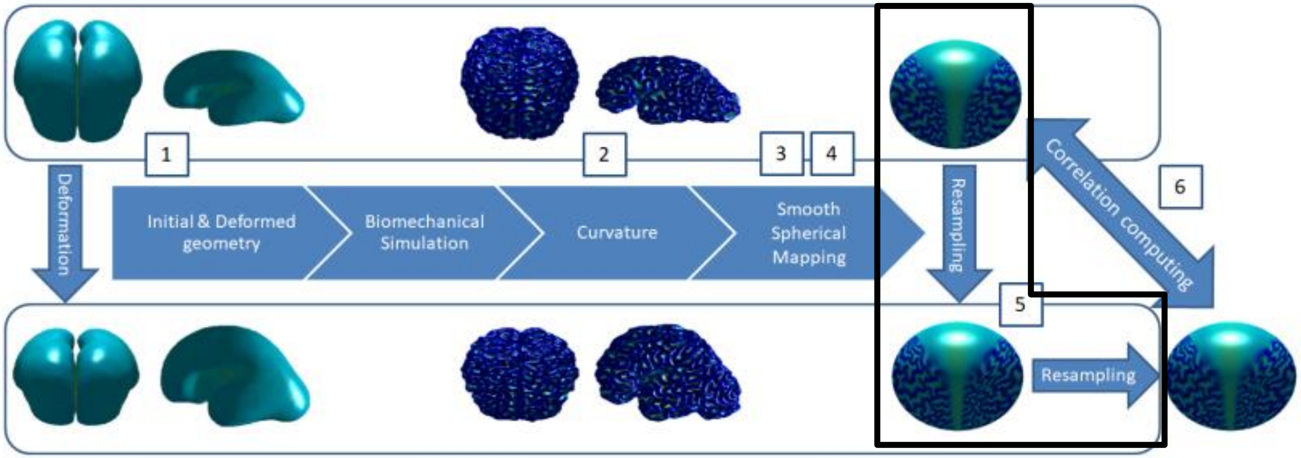

STEP 6:

Measure the similarity between the curvature of the surface $S_{ref}(t)$ and the resampled one of the surface $S_{a,b}(t)$.

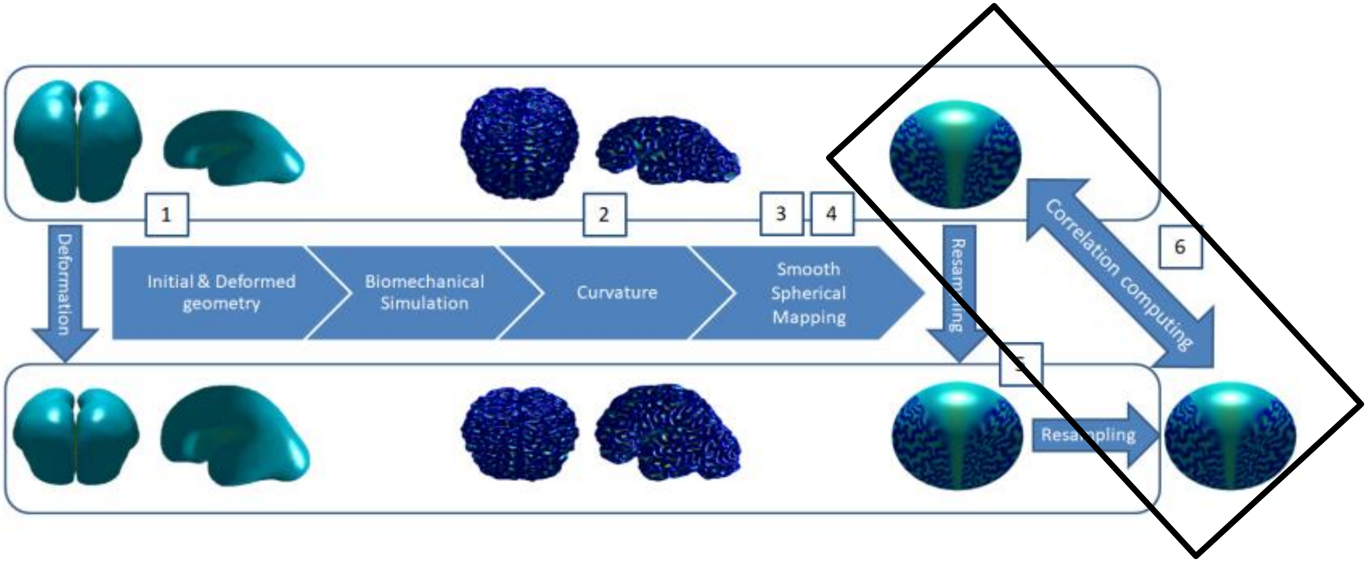

Results 1

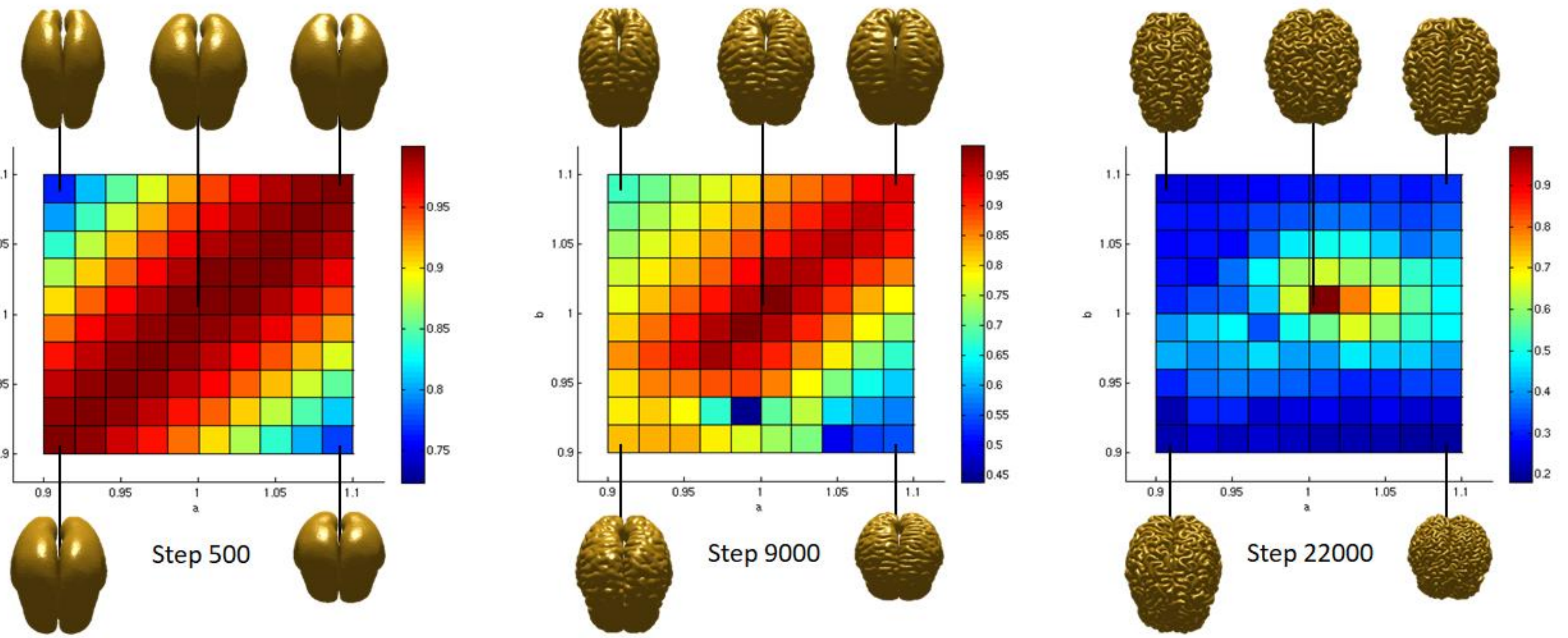

Correlation values for different scale factors at step 500, 9000 and 22000. *A. Bohi et al. 2019*

Results 1

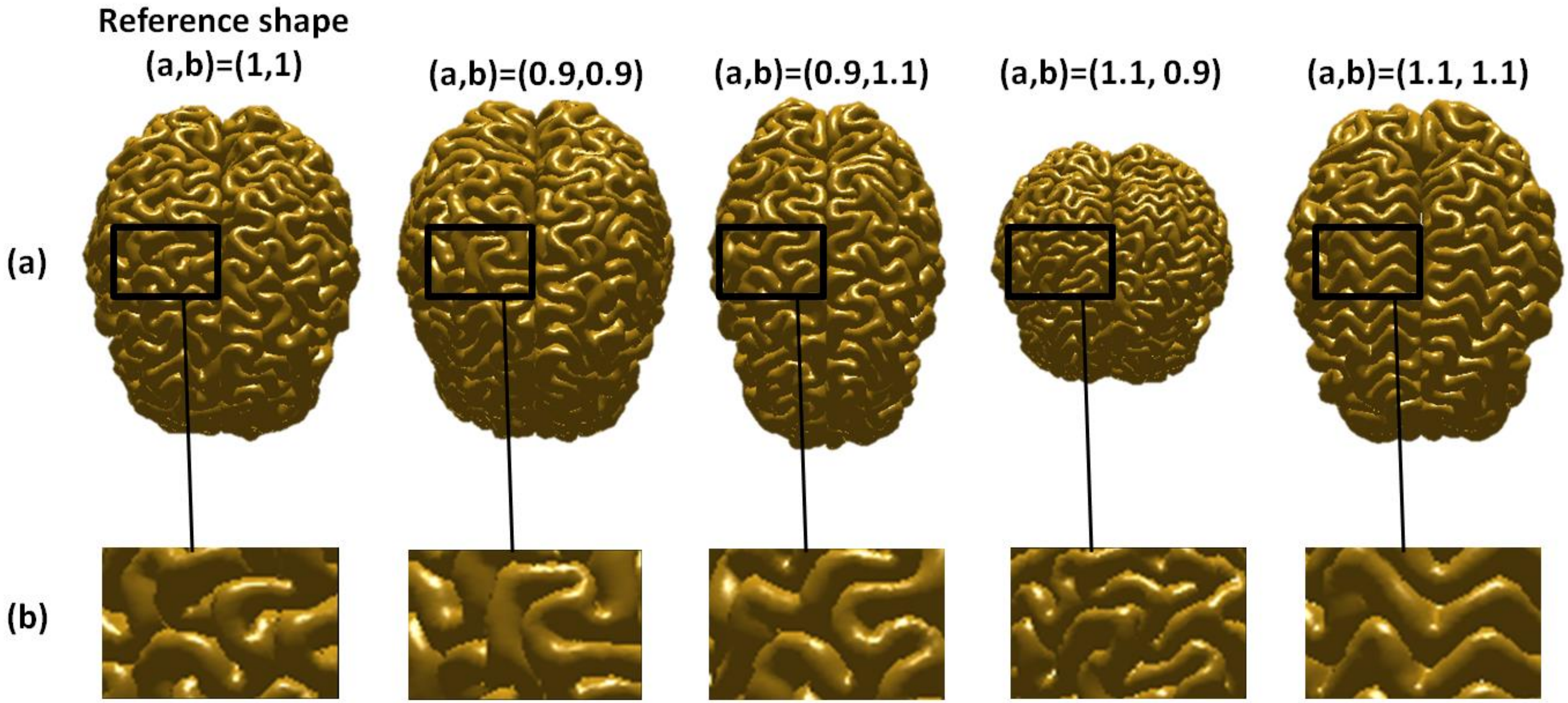

Variations in shape, size, placement and orientation of cortical folds across simulations.
A. Bohi et al. 2019

Results 2

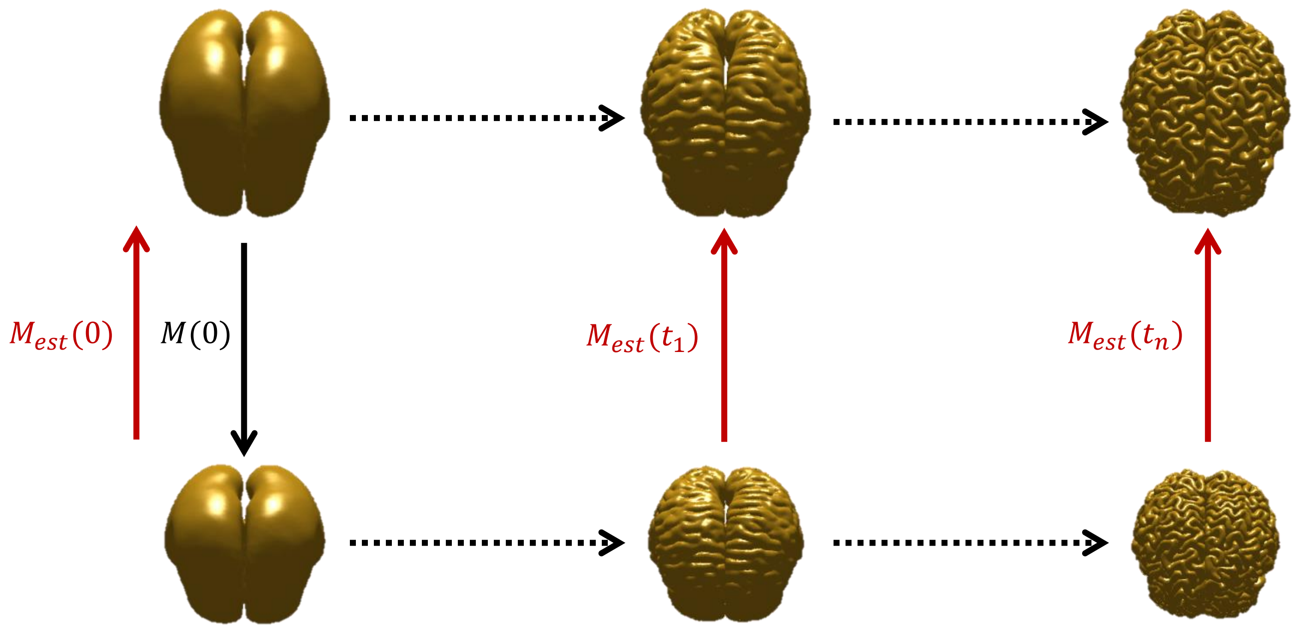

$$\|M_{est}(t) - M^{-1}(0)\| \leq 2.5\%$$

The biomechanical model preserves the global shape of the brain, in spite of appearance of cortical folding patterns

Conclusion:

The variations in the initial geometry of the brain strongly influence the cortical folding patterns in terms of shape, size, placement and orientation of cortical folds

Future works:

- Comparing simulated cortical surfaces with real ones
- Studying the impact of some neurodevelopmental disorders

Works in progress: Comparative study of methods for estimating curvatures

- **A number of general and specific shape analysis measures, derived from differential geometry, have been proposed to describe quantitatively the geometry of the cortical surface:**
  - **Folds depth and convexity estimation (*Rabiei et al. 2019*)**
  - **Gyrification index (*Rabiei et al. 2016*)**
  - **Spectral analysis (*Germanaud et al. 2012*)**

- **All surface processing pipelines, especially, neuroimaging tools dedicated to cortical shape analysis include a curvature estimation tool (FS, Caret, Brainvisa, ….)**

- **In the neuroimaging community curvature has long been used as a way to visualize the folded structure of the brain.**

→ No quantitative comparison study exists for assessing potiential differences across these techniques in terms of accuracy and robustness.

Works in progress : Comparative study of methods for estimating curvatures

- 7 methods for estimating curvatures are compared:
  - 5 from literature : Patch fitting methods (*Petitjean 2002*), Finite-differences methods (*Rusinkiewicz 2004*), Integral methods(*Taubin 1995*), Normal Cycles-based methods (*Steiner & Morvan 2003*) and Circular arcs-based methods (*Dong 2005*)
  - 2 included in neuroimaging tools (Caret and Freesurfer)

- Comparison on :
  - Synthetic surfaces (quadrics), directly with analytical curvatures
  - Real brains, by computing the robustness of methods in terms of reproducibility (Test-Retest protocol, 20 KKI subjects, 19 OASIS subjects)

- In both cases, measuring the sensitivity of methods against smoothing.

Curvatures on test-retest left hemisphere:

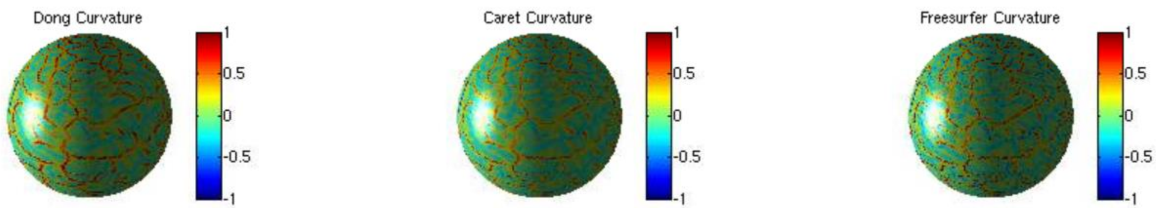

TEST MR1

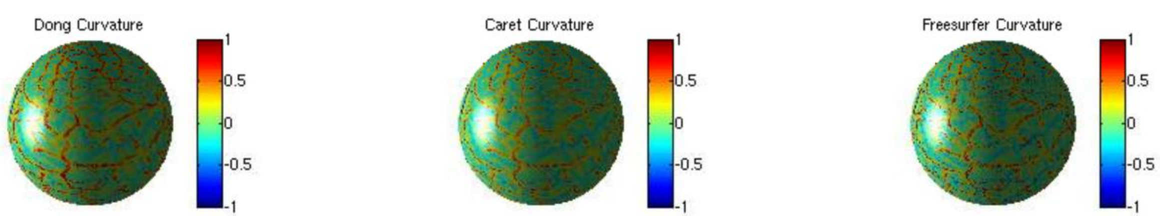

RETEST MR2

Curvatures on test-retest right hemisphere:

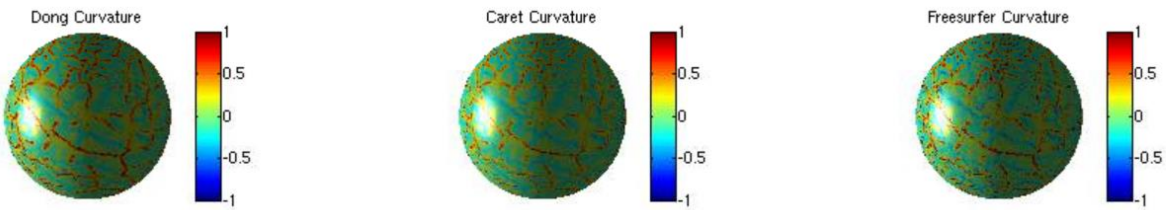

TEST MR1

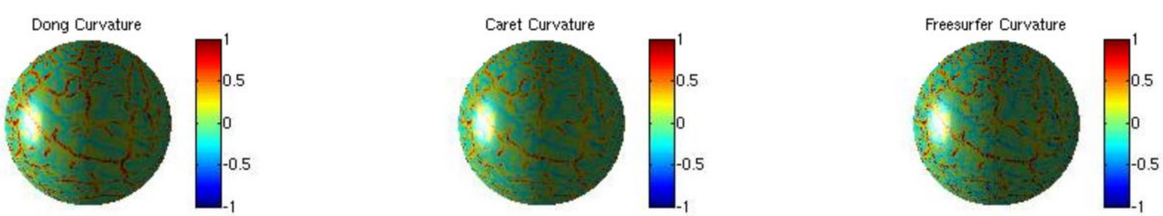

RETEST MR2

Some Preliminary Results: Before smoothing

KKI Subjects

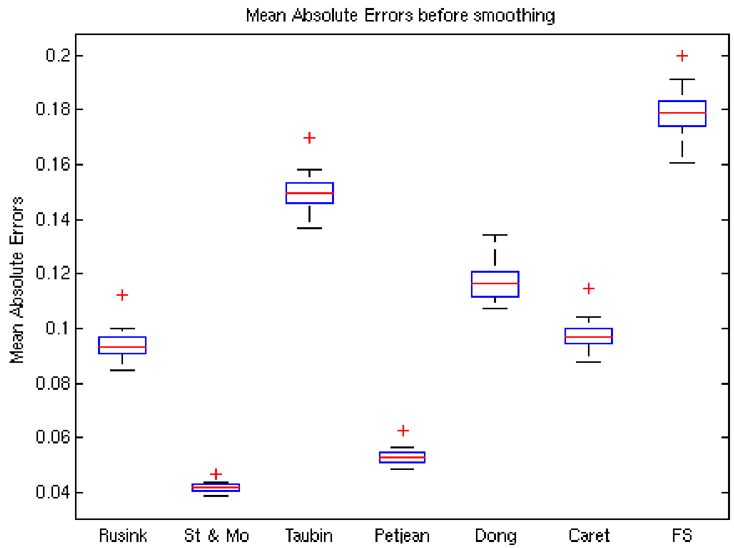

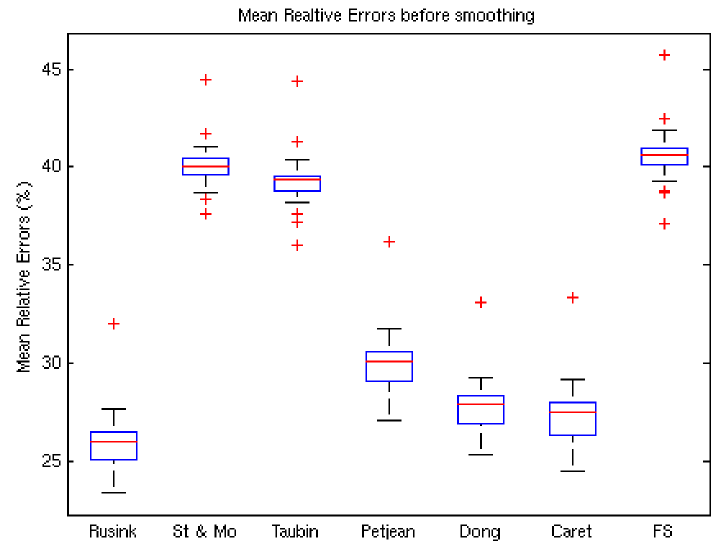

OASIS Subjects

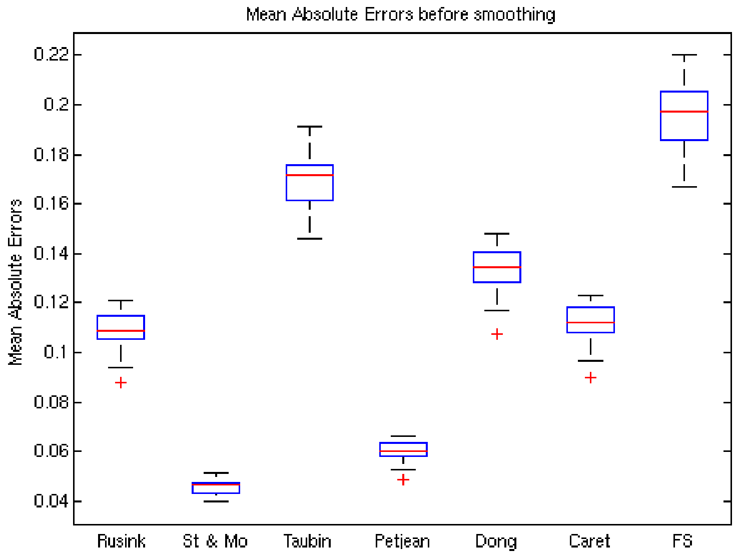

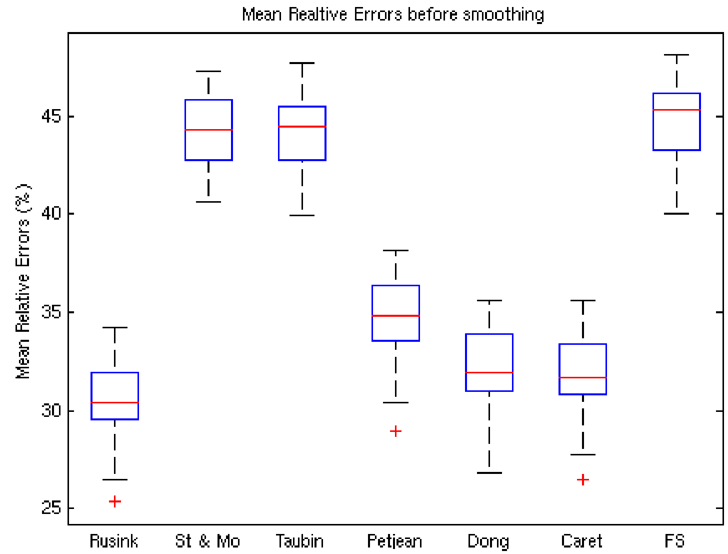

Some Preliminary Results: After smoothing

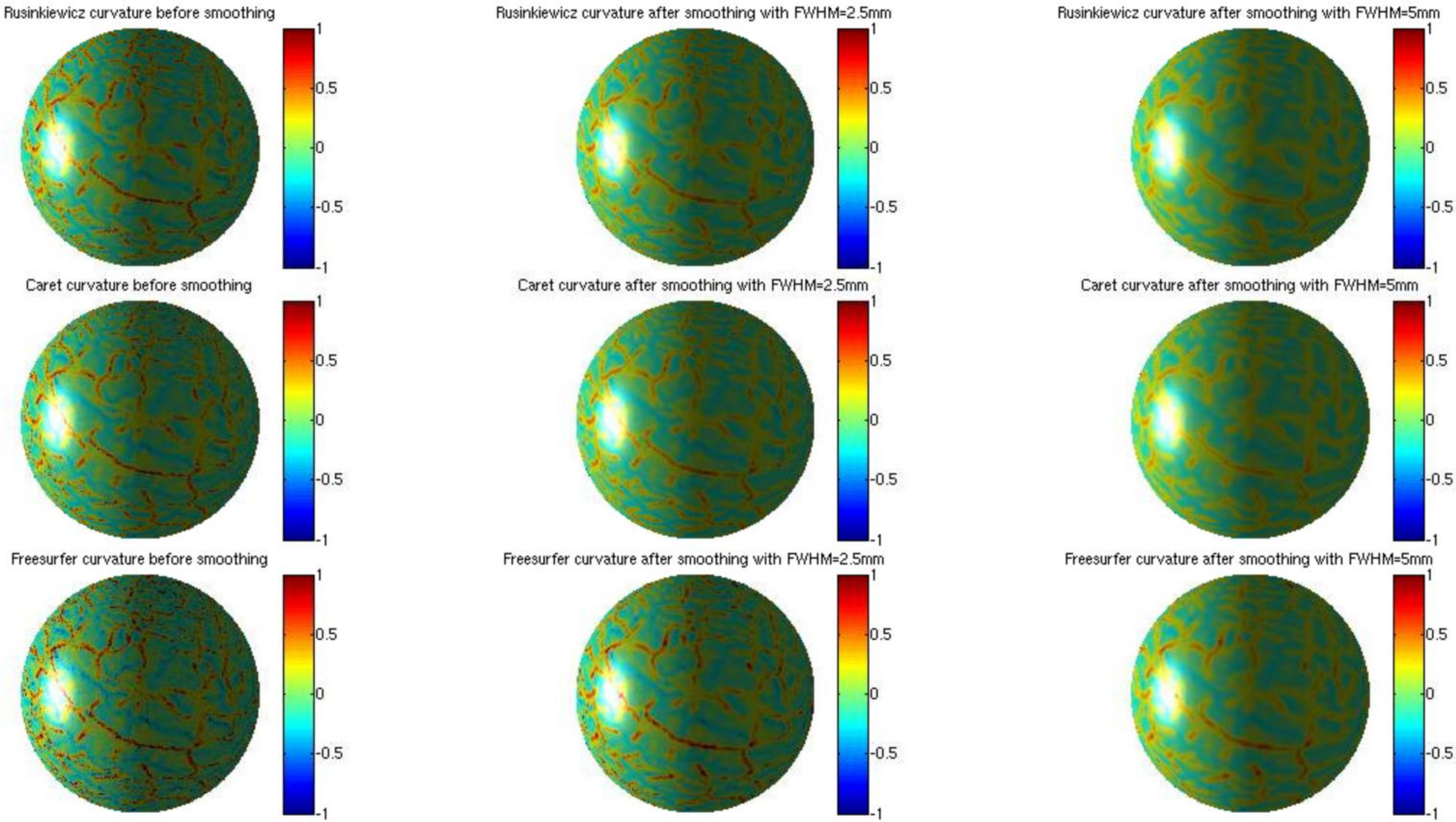

Some Preliminary Results: After smoothing

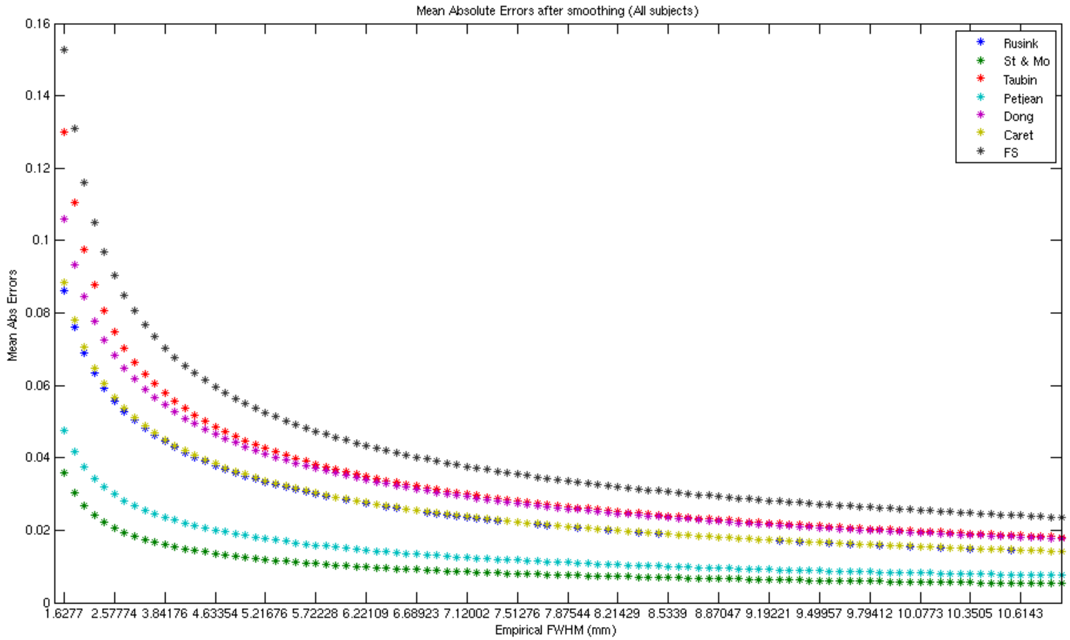

Mean Absolute Test-Retest Errors All Subjects

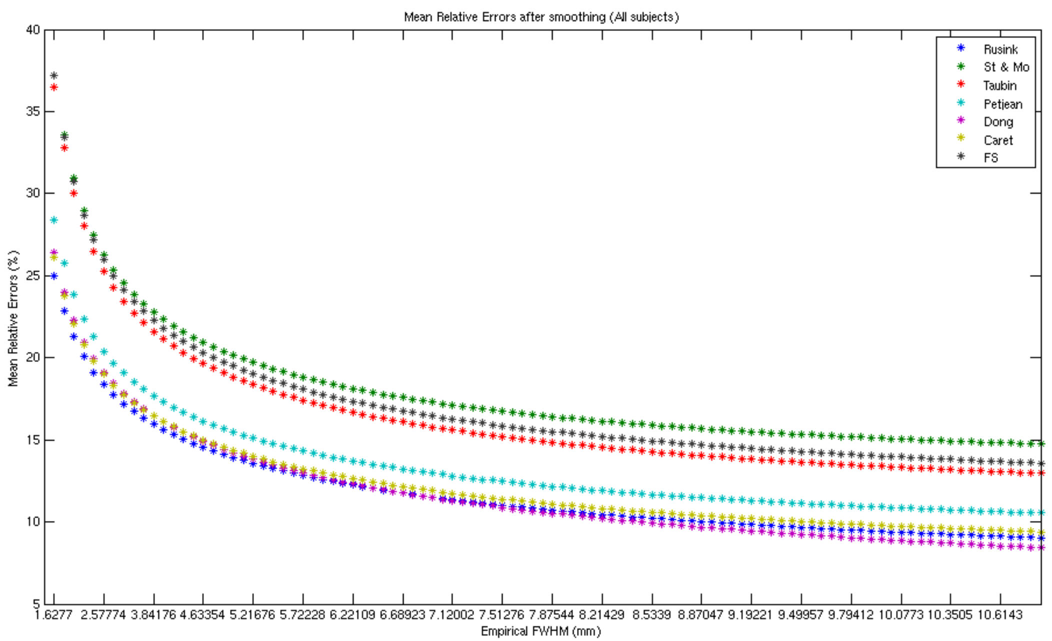

Mean Relative Test-Retest Errors All Subjects

Acknowledgments

- Julien Lefèvre
- Guillaume Auzias
- François Rousseau
- Xiaoyu Wang
- Mariam Al Harrach
- Mickael Dinomais

FONDATION RECHERCHE MÉDICALE

Thank You !

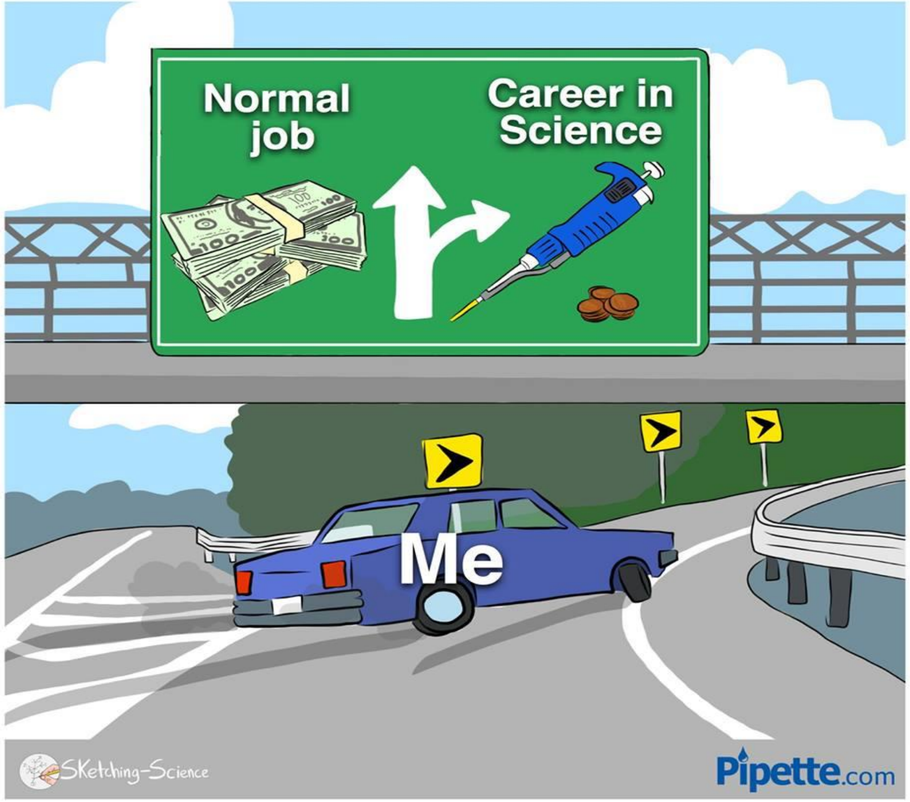

The value of science is more than money !
Do you agree ?

Annexe

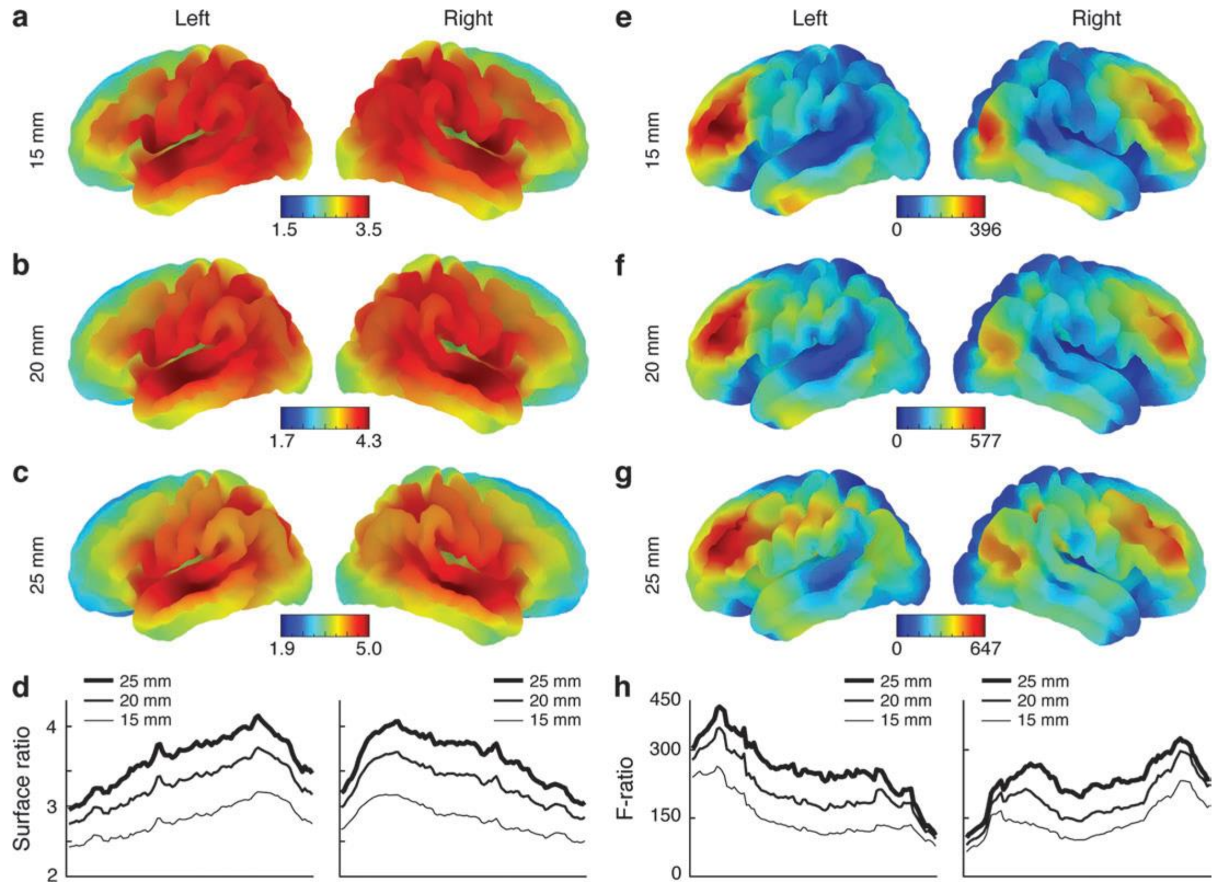

<u>Effect of sphere radius length</u>. The rostro-caudal gradient in the degree of folding, and the prefrontal effect of total cortical surface on folding, are the same for surface ratios computed with a sphere-radius of 15mm, 20mm and 25mm. *Toro et al. 2008*

Annexe

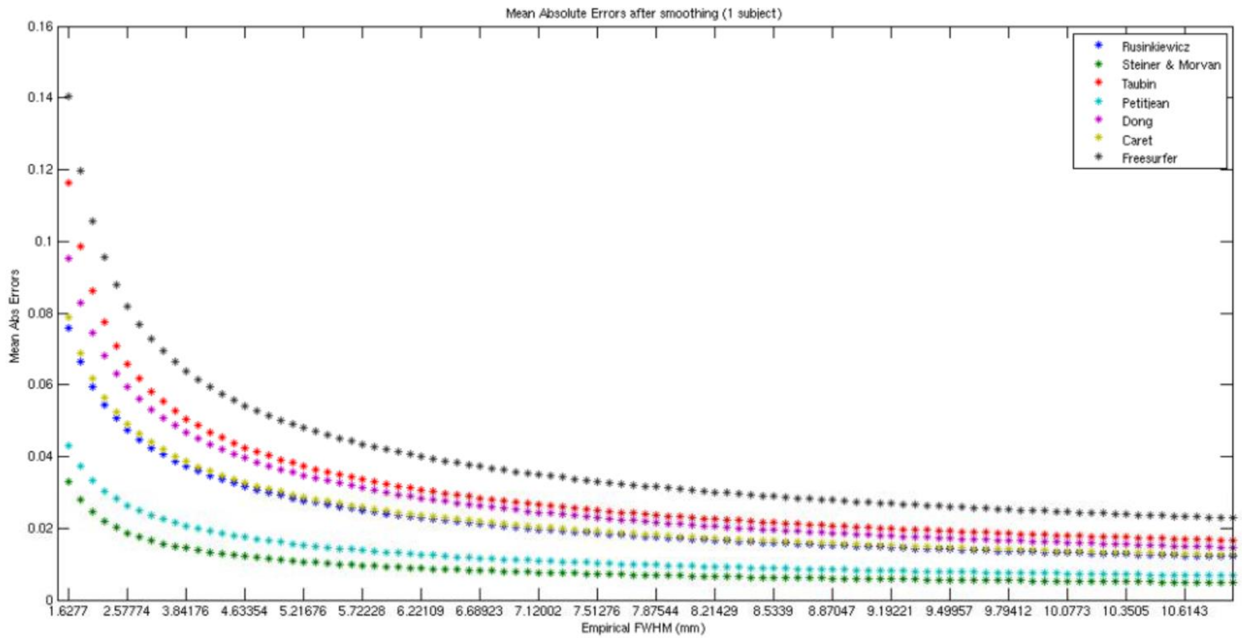

Mean Absolute Test-Retest Errors 1 subject

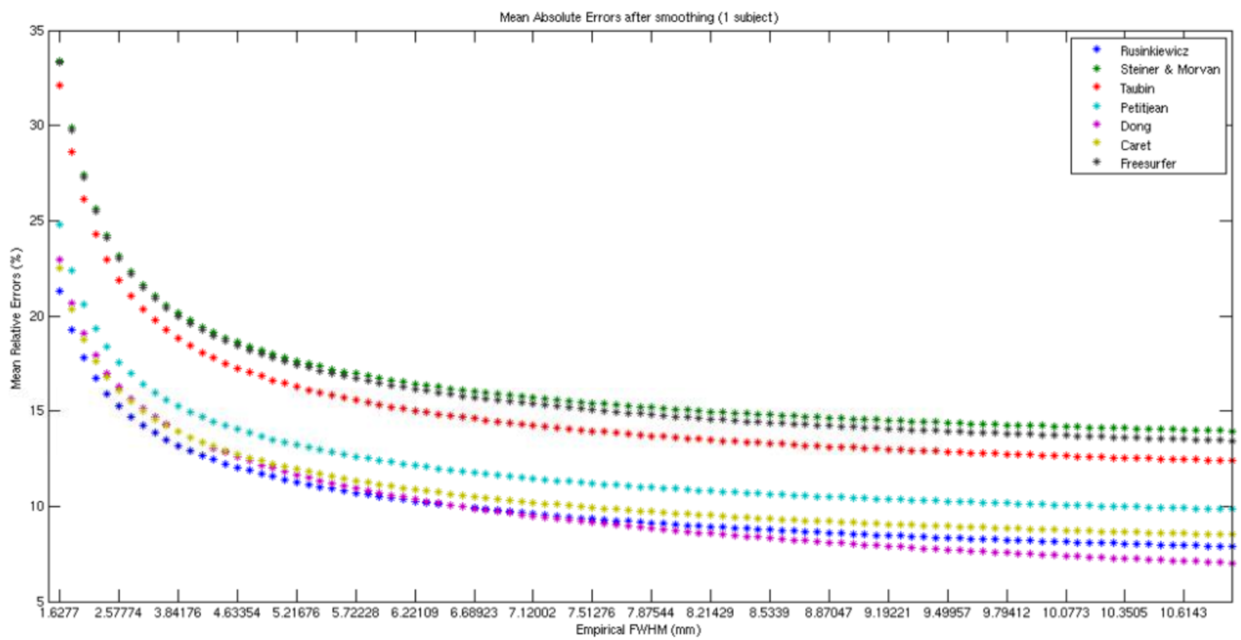

Mean Relative Test-Retest Errors 1 subject